# Product Development Team
# for
# NEXRAD Enhancements

## Quarterly Report – 3rd Quarter FY 02

**02.6.2 Polarization and Frequency Diversity**

*Continue development of algorithms that utilize polarization data to detect regions and fields of hydrometeors and non-hydrometeors, particularly those that are hazardous to aviation operations.*

a) Current Efforts

**(NSSL):**

**1. Polarimetric radar data collection and dissemination**

02.6.2.6 Begin real time testing of the HCA with the Cimarron polarimetric radar and provide real time polarimetric data and products to the Norman WSFO, start 1 Oct 01.

Several years of effort on the NOAAs research WSR-88D radar culminated in the generation and display of dual polarization data late this spring. For expediency the system was configured from several autonomous subsystems, most of which were not specifically designed for the project. Therefore, integration entailed significant ingenuity and resourcefulness. First, a custom frequency-offset generator, to produce two intermediate frequency (IF) signals, was designed. A manufacturer built this hardware and NSSL installed and connected it to the Sigmet RVP7 processor. The Sigmet processor requires the two offset IF signals, and is connected in a passive mode to the radar. Software was developed to transfer Sigmet data onto the local area network so that it could be further manipulated to produce hydrometeor classes and rain amounts. These products were then provided to the NWS forecasters for evaluation. The proposed polarization scheme uses simultaneous transmission and reception of horizontally and vertically polarized echoes. Because it has not been tested, we have devoted much time to engineering evaluation and calibration.

Polarimetric algorithms to process the raw data and generate hydrometeor classification and rainfall estimation products were developed for the NSSL Warning Decision Support System-Integrated Information (WDSS-II) display system. During the spring of 2002, polarimetric KOUN radar data were collected for several precipitation systems. Fig. 1 shows KOUN reflectivity (Z), differential reflectivity (ZDR), correlation coefficient (rHV), differential phase

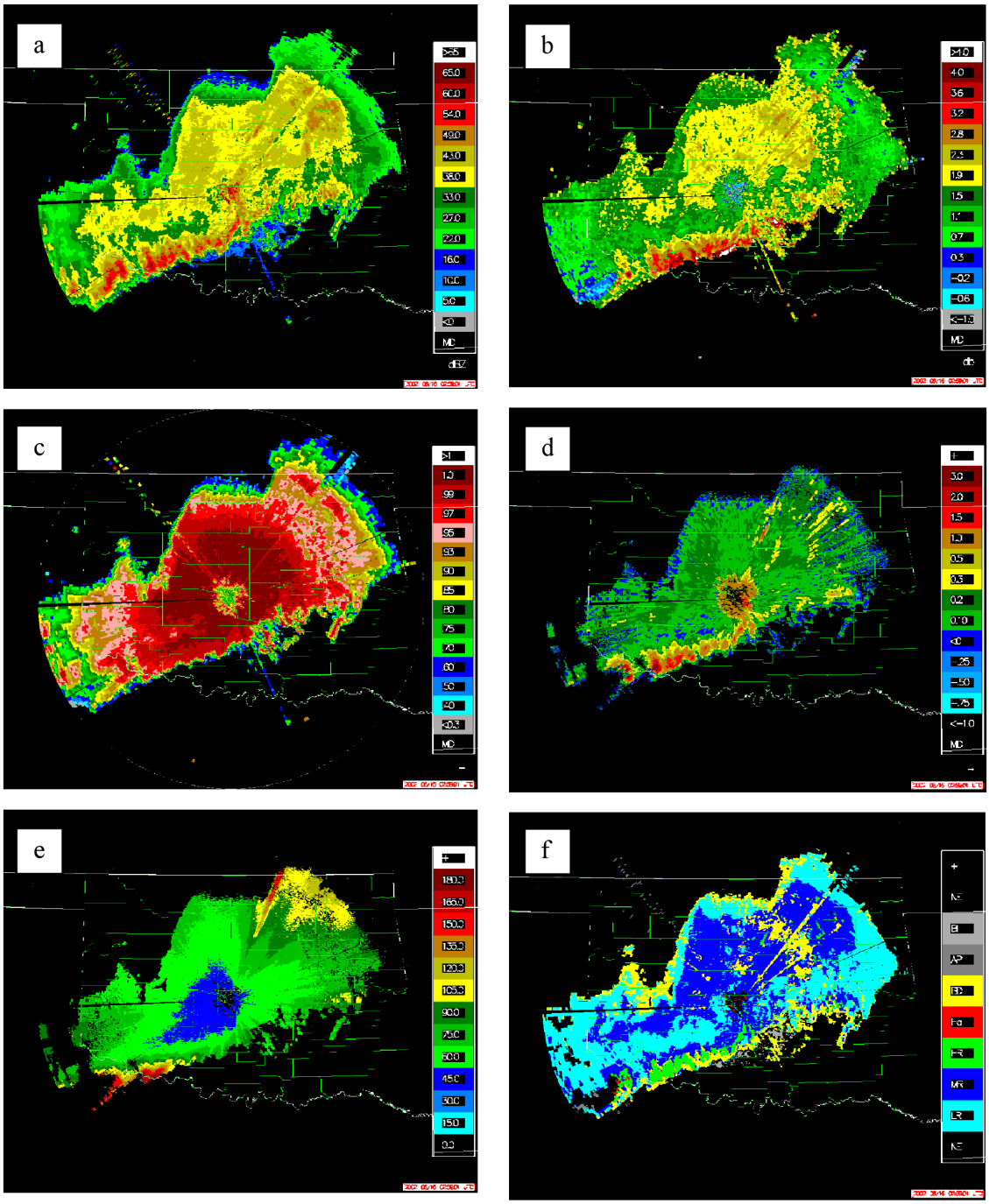


Figure 1. KOUN WSR-88D a) reflectivity, b) differential reflectivity, c) correlation coefficient, d) specific differential phase, e) differential phase, and f) polarimetric hydrometeor classification for the June 16, 2002 MCS at 0300 UTC. The HCA used for these early tests has 5 meteorological and 2 non-meteorological categories. The meteorological categories include 1) light rain (LR), 2) moderate rain (MR), 3) heavy rain (HR), 4) hail (Ha), and 5) big drops (BD). The non-meteorological categories include 1) anomalous propagation (AP), and 2) birds and insects (BI).

(FDP), specific differential phase (KDP), and results from the Hydrometeor Classification Algorithm (HCA) for an MCS that passed through central Okla-

homa on 16 June 2002. The HCA used for this operational test has 5 meteorological and 2 non-meteorological categories. The meteorological categories include 1) light rain, 2) moderate rain, 3) heavy rain, 4) hail, and 5) big drops. The non-meteorological categories include 1) anomalous propagation, and 2) birds and insects. These data and products were displayed in real-time at the Norman, Oklahoma National Weather Service Office. During the event, an NSSL observer assisted NWS forecasters in the analysis of the dual polarization data and products.

The 0.5° base scan data in Fig. 1 extends to a range of approximately 300 km. At this time, the MCS was beginning to enter its dissipative stage, with the convective line still producing heavy rainfall but very little hail. The region of heavy rainfall, as indicated by both large reflectivities and specific differential phases along the convective line, are clearly evident in the HCA output (Fig. 1f) in the SW corner of OK. The HCA also indicates an extensive region classified as "big drops" along the leading edge of the convective line. This feature is particularly evident in SW Oklahoma, where differential reflectivities at the leading edge of the convective line often exceed 4 dB. Regions of big drops are common features at the leading edge of convective cells. Our ground-based observations with a video disdrometer indicate that the large reflectivities associated with these large, but relatively sparse drops can often lead to overestimation of rain by as much as a factor of ten if a Z-R relation is used. An extensive region of light to moderate rain is indicated by the HCA in the MCS trailing stratiform region.

A region of big drops is also indicated by the HCA in NW Oklahoma. When comparing this region to the large differential reflectivities in Fig. 1b and low correlation coefficients in Fig. 1c, it is clear that this "big drop" feature is an indication of large, wet aggregates that are associated with the stratiform bright band. Our experimental 11 class HCA, which includes several ice categories, has a bright band category that indicates this feature quite well. This classification scheme will be added to the suite of real-time polarimetric KOUN algorithms this fall after additional refinement and testing is completed. At ranges beyond the bright band feature, the differential reflectivity decreases and correlation coefficient increases, indicating a deep region of dry snow/ice at levels above the bright band.

Another feature seen in several panels of Fig. 1 (particularly the hydrometeor classification shown in Fig. 1f) is a sector of severe blockage at approximately 40° azimuth. For this case, the blockage is caused by the NWS test and development KCRI radar, which is located approximately 250 m to the NW of the KOUN radar. Blockage represents a significant rainfall estimation problem for several regions of the country, particularly in the mountainous western states. Fig. 2, however, shows how these rainfall estimation problems can be mitigated by polarization estimation techniques, which are largely immune to blockage. Fig. 2a shows 3-hour rainfall accumulation using the standard NWS Z-R rela-

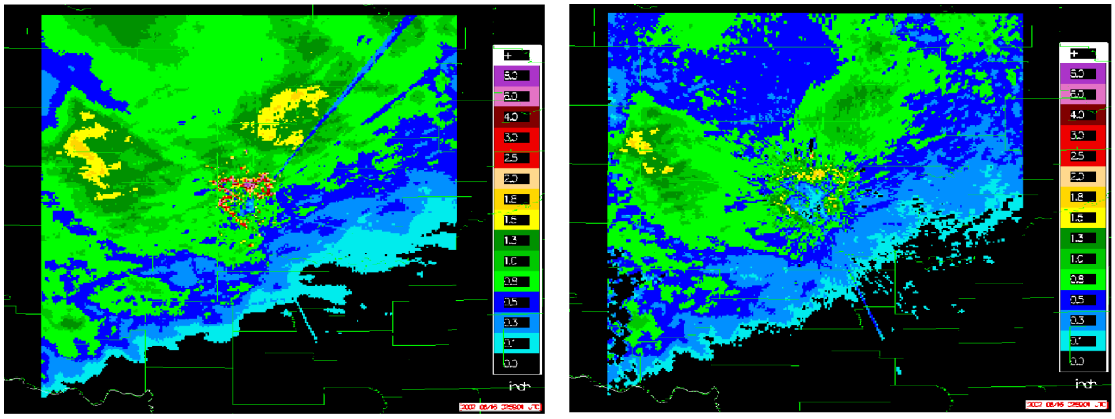

Figure 2. KOUN WSR-88D 3 hour rainfall accumulation using a) a Z-R relation, b) polarimetric KDP relation.

tion; Fig 2b. shows 3-hour rainfall accumulation using a polarimetric KDP relation. In addition to demonstrating better overall agreement with ground-based observations obtained from Oklahoma mesonet stations (not shown), the comparison clearly shows the relative immunity of the polarimetric estimator to blockage.

The utility of using polarimetric radar to identify regions of hail was also well demonstrated by data collected in the 16 June 2002 MCS. Fig. 3 shows KOUN reflectivity (Z), differential reflectivity (ZDR), correlation coefficient (rHV), and results from the Hydrometeor Classification Algorithm (HCA) for a hail core in NW Oklahoma at 0045 UTC, a time at which convection in the leading line was at its most intense stage. At times, reflectivities associated with this hail core reached 69 dBZ. The most notable polarimetric feature associated with this intense hail core, as identified by the HCA (Fig. 3d), is a significant local minimum in the differential reflectivity (Fig. 3b) in a region that appears to be collocated with the highest reflectivity core. This region is also characterized by a significant drop in the correlation coefficient (Fig. 3c).

## 2. Planning for the Joint Polarization Experiment (JPOLE)

02.6.2.4 Conduct a workshop on polarimetric measurements of precipitation in anticipation of JPOLE, start 15 May 02.
02.6.2.E4 Report on results 15 June 2002.

In addition to the polarimetric KOUN data collection and delivery associated with the Joint Polarization Experiment (JPOLE) operational demonstration, significant effort over the past three months was also devoted to planning for the JPOLE field campaign (proposed for the Spring if 2003). During the JPOLE field campaign, scientists from a number of universities and governmental agencies are seeking to conduct an intense observational period to collect data sets that can be used to advance numerous scientific objectives and better test

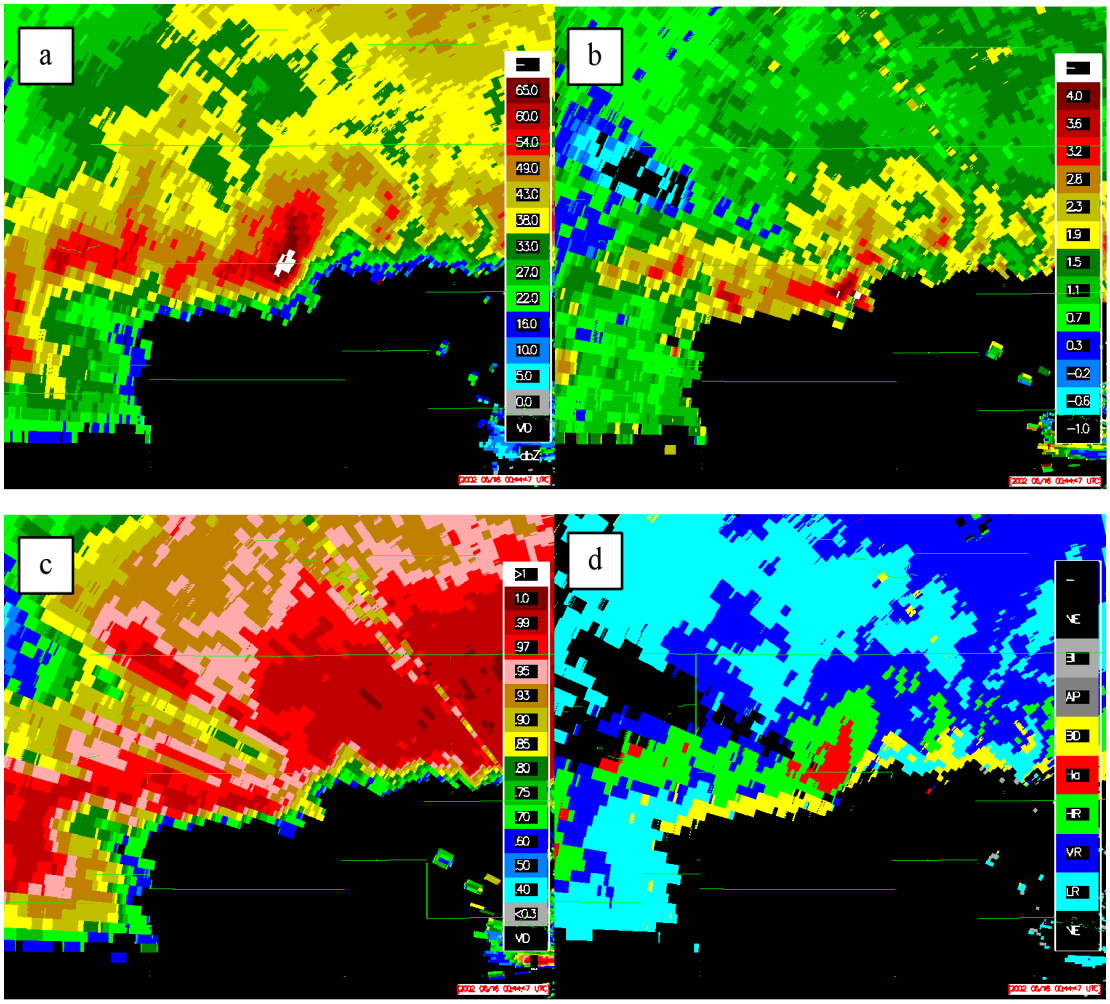


Figure 3. KOUN WSR-88D a) reflectivity, b) differential reflectivity, c) correlation coefficient, and d) polarimetric hydrometeor classification for the June 16, 2002 MCS at 0045 UTC.

the engineering design and data quality of the polarimetric KOUN WSRR-88D radar. In support of JPOLE field campaign planning, a Science Overview Document and facility requests for the Colorado State University CHILL polarimetric radar and South Dakota School of Mines and Technology T-28 aircraft (as well as 8 scientific proposals from collaborators at 6 universities) were submitted to the National Science Foundation in the past 3 months. A presentation in support of this project was also made to NSF by Dr. Terry Schuur of the University of Oklahoma/Cooperative Institute of Mesoscale Meteorological Studies and Dr. V. Chandrasekar of Colorado State University/Department of Electrical Engineering. A summary of JPOLE operational demonstration and field campaign objectives, as well as copies of the science overview document and facility requests, can be found on the JPOLE web site, located at: http://www.nssl.noaa.gov/JPOLE/. These documents constitute the deliverable.

**(NCAR)**:

02.6.2.11 Continue development of NCAR freezing level algorithm. Start 1 Oct 01. Due: 30 September 02.

The NCAR freezing level algorithm was applied to a long-lived event observed as part of the IMPROVE-II field program conducted in the Oregon Cascade mountains during November and December of 2001. The measurements were collected with NCAR's S-Pol radar. Verification data are available from nearby National Weather Service soundings, special rawinsonde releases, and aircraft.

Freezing level designations have been made with the radar reflectivity, linear depolarization ratio, and correlation coefficient measurements. A typical vertical profile of these measurements and differential reflectivity is shown in Fig. 4.

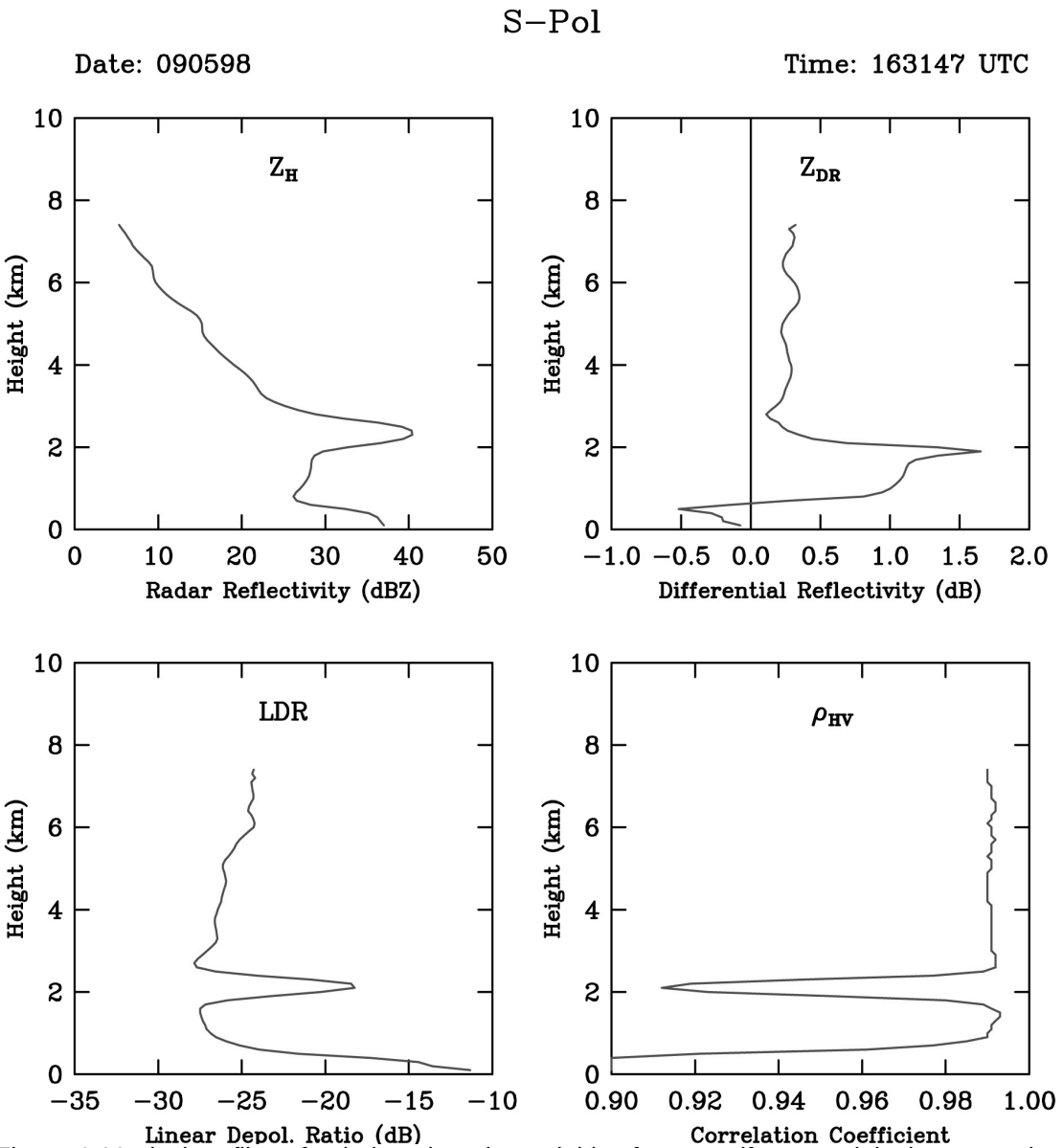


Figure 4. Vertical profiles of polarimetric radar variables for a stratiform precipitation event during IMPROVE-II. Ground clutter contaminates the measurements below 0.8 km.

The algorithm relies on statistical relationships between parameter extremes in the melting layer and the 0C level. Small climatological differences are being found for different geographical regions and seasons. The melting layer is readily apparent in the radar reflectivity, linear depolarization ratio, and correlation coefficient profiles. The ensemble designated freezing level is 2.80 km.

Algorithm designations on a 5 km grid to the east of the radar are presented in Fig. 5. The results are overlaid on a PPI at 1.5 degree antenna elevation. Vol-

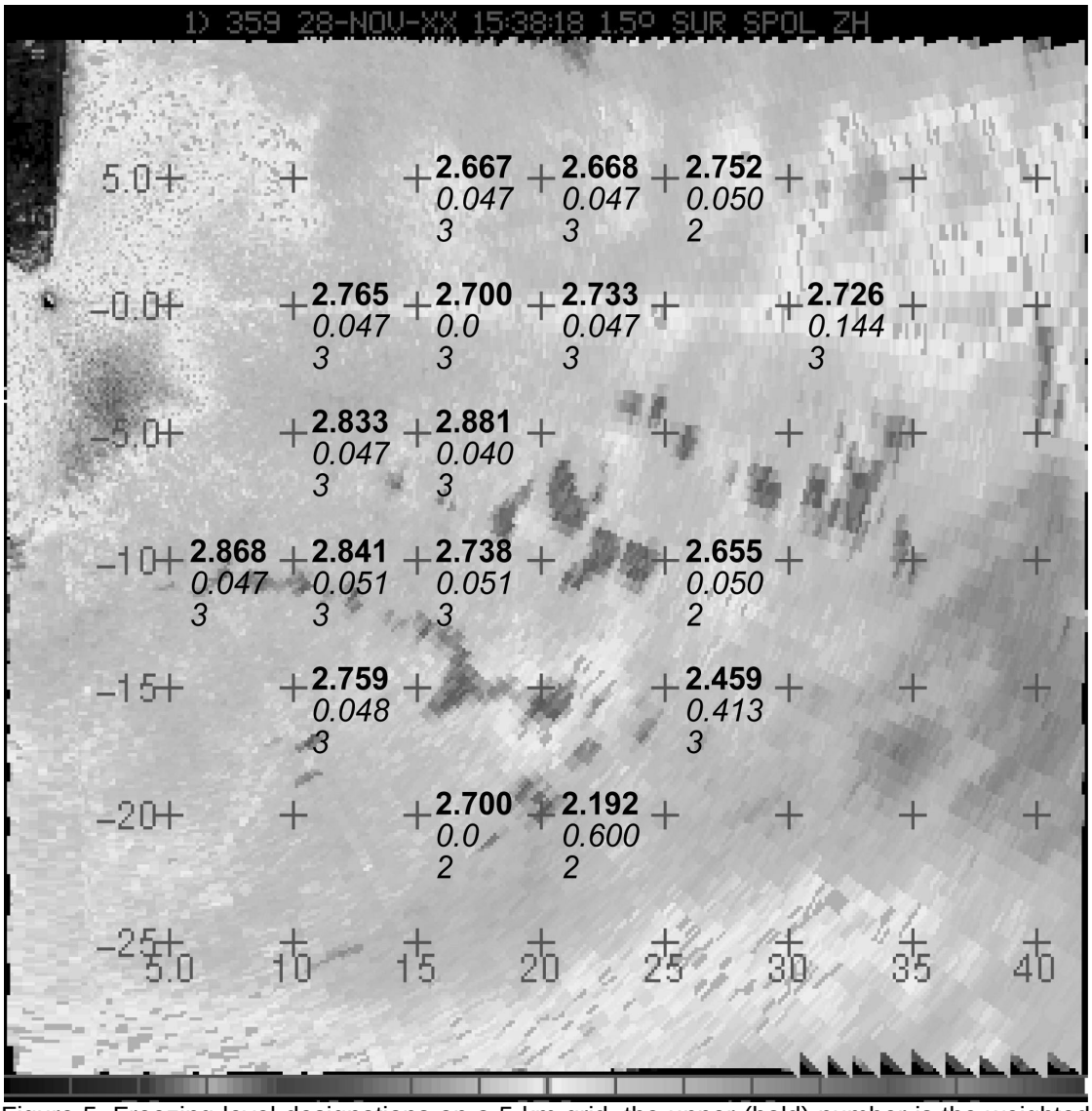


Figure 5. Freezing level designations on a 5 km grid. the upper (bold) number is the weighted freezing level height based on the ensemble of measurements. The middle number is the standard deviation among the individual parameter designations. the number of parameters meeting melting layer model correlation criteria is also given.

umetric data were available only for the 80 to 140 degree azimuthal sector. An extended area of ground targets can be seen east through southeast of the

radar. Nevertheless, freezing level designations could be made over a broad area. The uppermost number is the ensemble freezing level estimate. For quality assessment the standard deviation of the individual parameter estimates and the number of parameters for which an estimate could be made are also shown. The two outlier heights in the southeast show large standard deviations. Parameter profiles which do not correlate with the model are not considered.

Figure 6 shows mean and median designations made with the various parame-

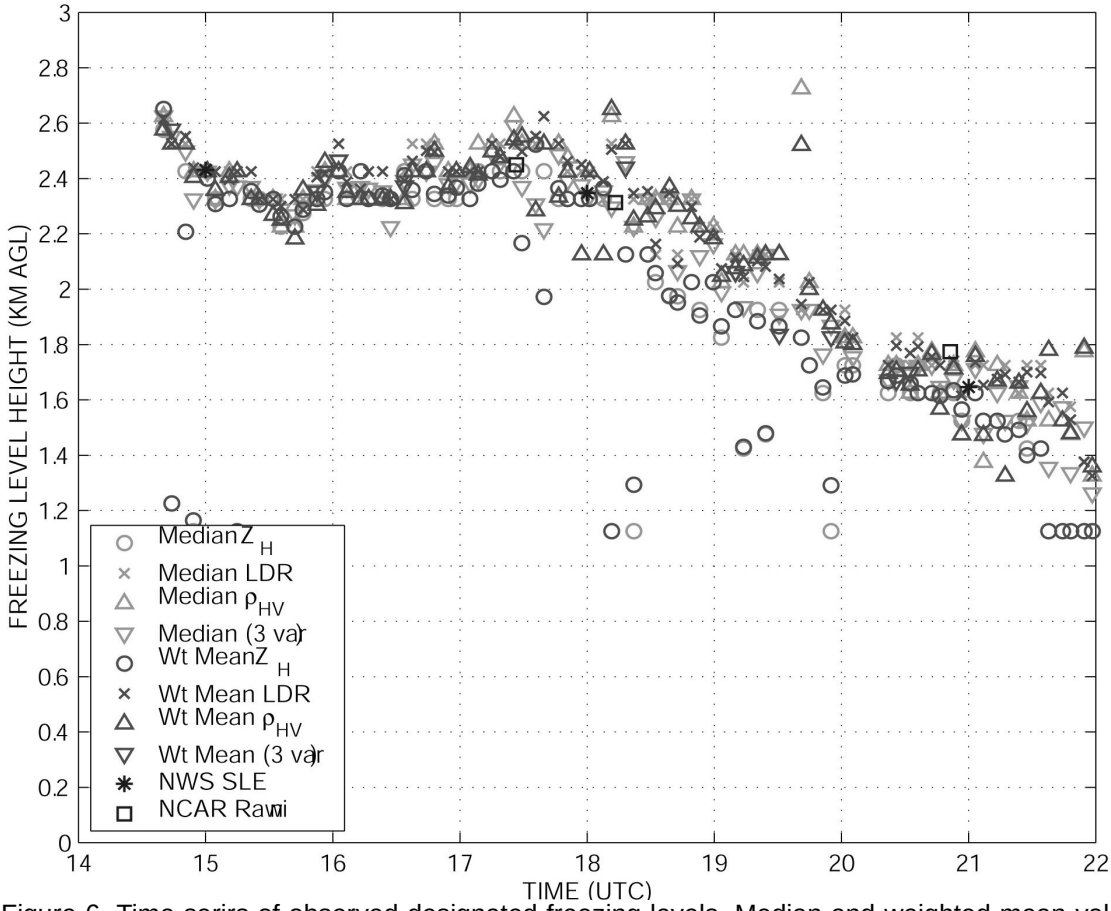


Figure 6. Time serirs of observed designated freezing levels. Median and weighted mean values are shown for the three polarimetric parameters and for the ensemble designations.

ters and combinations thereof for an 8 hour period. Verification data are also given. With time the freezing level lowers by about 1.2 km. Most outliers are with radar reflectivity. Also, the scatter increases with time as the freezing layer lowers and ground targets exert more influence on the results.

Accurate freezing level determination is requisite for hydrometeor classification. Also, the information is important for isolating regions of potential icing hazard.

02.6.2.12 Verify non-precipitation and hydrometeor components of the HCA. Start 1 May 02. Due: 30 Sep 02.

Hydrometeor classifications for the 5 September 1998 event in Florida are being examined. In particular interrelationships among ice crystal types, bright band characteristics, and rain drop distributions are being studied.

Key task activities during the quarter appear in monthly reports for April and May. Scientific findings regarding rain-snow discrimination and drop-size distribution retrieval were summarized in papers presented at the 10th Conference on Aviation, Range, and Aerospace Meteorology and the 11th Cloud Physics Conference.

We continue to wait for the processing of the hydrometeor observations for IMPROVE-II.

d) Interface with other Organizations

None.

e) Activity Schedule Changes

None.

**02.6.3 Circulations**

*Display the NSSL Mesocyclone Detection Algorithm (MDA) and Tornado Detection Algorithm (TDA) output to Corridor Integrated Weather System users to establish utility for Terminal Convective Weather Forecast (TCWF) and National Convective Weather Forecast (NCWF) aviation users.*

a) Current Efforts

No progress to report. Task is set to begin 01 Aug 02.

b) Planned Efforts

To begin 01 Aug 02.

c) Problems/Issues

None.

d) Interface with other Organizations

None.

e) Activity Schedule Changes

None.

**02.6.4 Technical Facilitation**

*Continue to develop software infrastructure and tools required for the development and testing and display of NEPDT algorithms.*

a) Current Efforts

The WDSS2 system was enhanced in several ways to support various research efforts at NSSL. These included support for new types of data and for new algorithms to process the data.

(1) Improvements were made to a merger process that merges data from different sensors in real-time. The WDSS-II display can now ingest and display the outputs of this merger process. Shown in Fig. 7 is a merger of three weather radars (from Tulsa, Hot Springs and Oklahoma City) on May 20, 2001 at 1km above the earth's surface. Fig. 8 shows the same coverage for 2km AGL. The interface includes a way to step up and down the various height levels. It is also possible to do 3D navigation and cross-sections of this merged grid.

(2) The K-Means clustering algorithm was enhanced to identify storms and provided growth and decay estimates and forecast products from radial data as well as from LatLon grids (such as the merger). Fig. 9 shows the products available from the algorithm. Fig. 10 shows the growth-and-decay product superimposed on the original reflectivity image. Fig. 11 kmeans_forecast.gif shows the 60min forecast field (storm core on the right) superimposed on the original image. Notice the predicted strengthening of the storm, as well as the advection.

(3) Allow products to have different colormaps depending on mode, so that for example, Reflectivity products have different colormaps depending on the VCP.

(4) Ingest and display of the new polarimetric radar (KOUN). Figs. 12, 13 and 14 show the hydrometeor classification, $\rho_{HV}$ and $Z_{dr}$ images from the polarimetric radar as visualized in WDSS-II.

(5) Bug fixes and continued development of TDWR data distribution and ingest.

(6) Continued development of LDM access, table, tracks and trend visualization (Fig 15).

7) A query interface was implemented, so that algorithm detections could be graphically filtered based on intermediate/final parameters, to enable setting of appropriate thresholds.

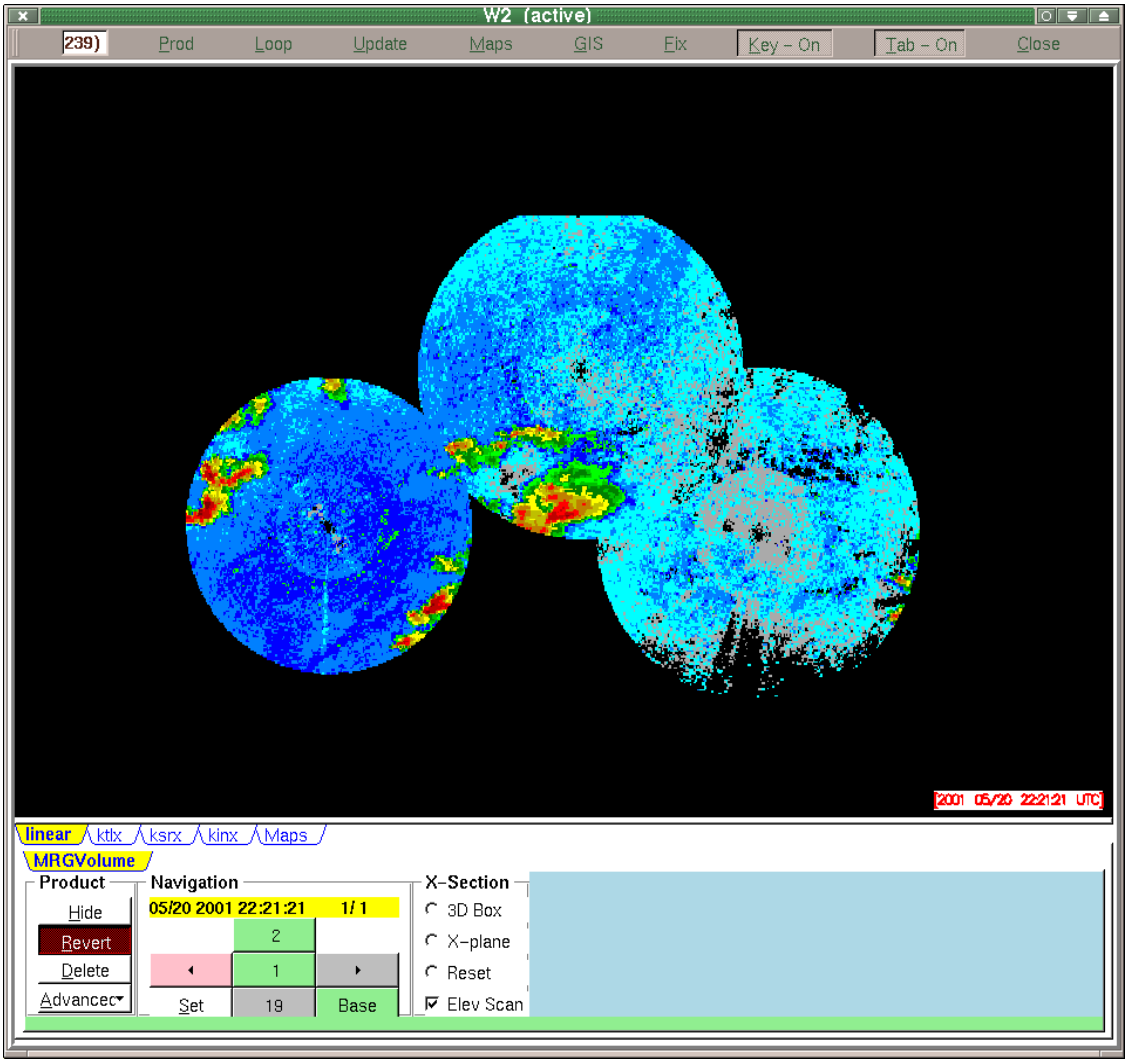


Figure 7. Example of 1 km AGL coverage of the Oklahoma City, OK, Tulsa, OK, and Hot Springs, AR, radars.

8) A way to over-ride system-wide configuration files with local ones was implemented. This enables algorithm developers to change colormaps, etc. to see features of interest.

(9) Displayed shapefiles of tornado path in WDSS-II, superimposed on algorithm detections for ground-truth verification. ground_truth.gif The map "may3" is shown by the white lines representing tornado path (Fig. 16).

(10) Started to work on multiple windows display (Fig. 17).

(11) Optimized read of database in real-time, to enable quicker startups.

(12) Implementated polar VIL and composite products that work on both TDWR and 88D data. These algorithms work in a rapid-update mode (Fig. 17 ).

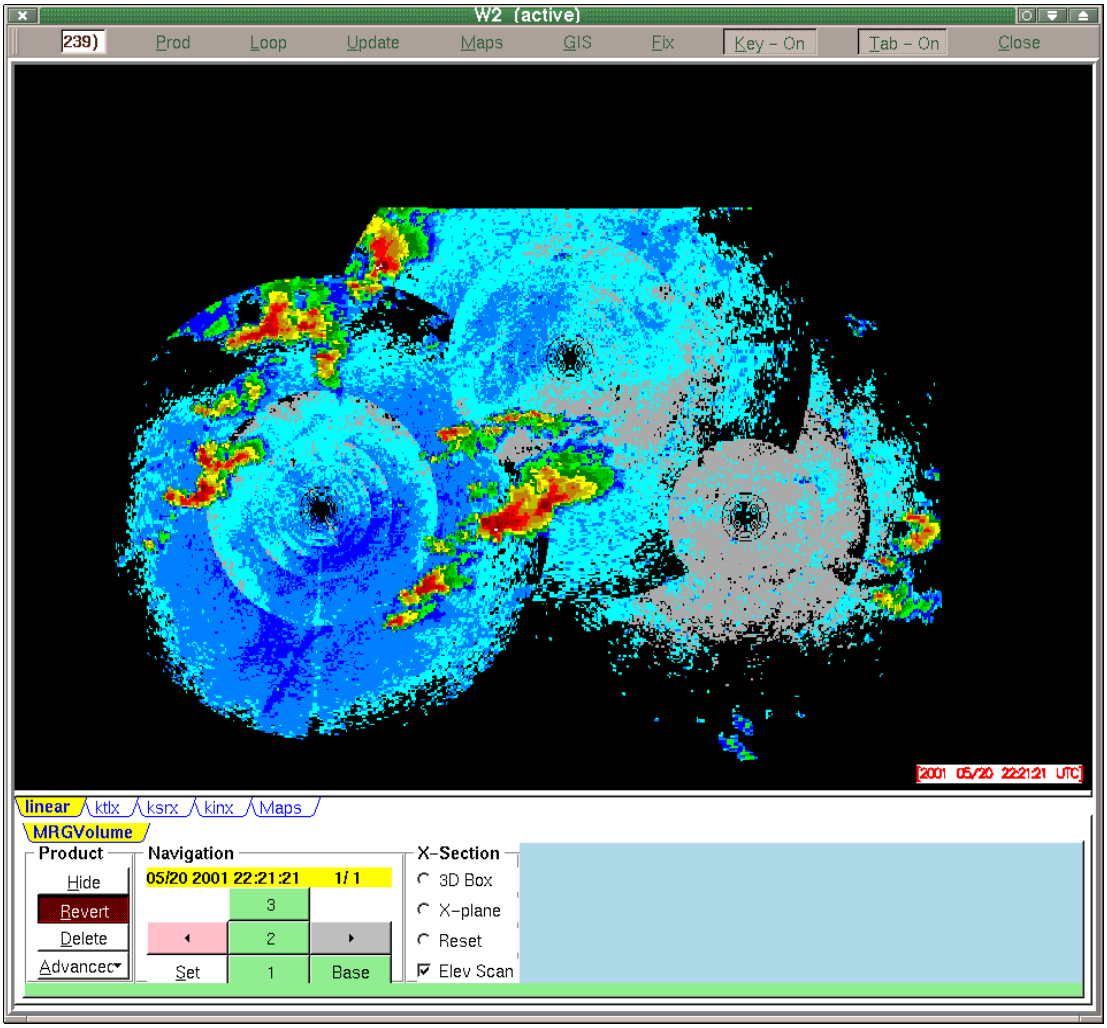


Figure 8. Same as Fig. 7, but for 2 km AGL.

b) Planned Efforts

Continue display interface and capability development and enhancement.

c) Problems/Issues

None.

d) Interface with other Organizations

None.

e) Activity Schedule Changes

None.

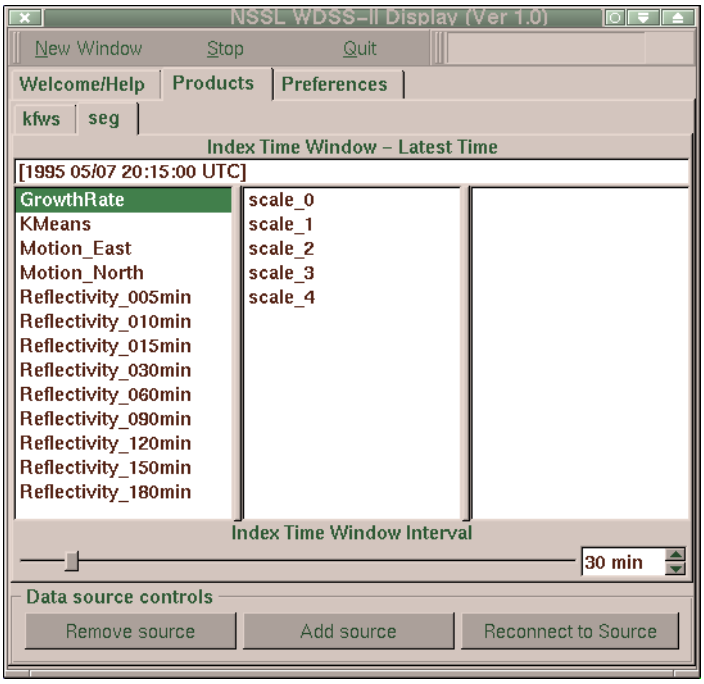


Figure 9. List of products avaialbel frome the NSSL k-means clustering algorithm.

### 02.6.9 Composite Products

*Composite Products - develop a high-resolution multi-radar product with nested resolutions from 500 m to 5 km, that runs in a large analysis domain (such as CIWS), and that is updated at no more than 240 s intervals.*

a) Current Efforts

Continued to develop code that converts TDWR data into an internal format for the bright-band identification and the 3-D multi-radar mosaic algorithms. The code assumes that the TDWR data have been organized and written into disk files. NSSL has developed software that collects real-time TDWR data from OKC airport via a T1 line, and combines and writes all radials from the same tilt into a file. The converter code reads in the files and extracts information such as tilt number, elevation angle, azimuth angles of each radials, etc. The code will also extracts and decodes the reflectivity, velocity, and other data fields from the file.

b) Planned Efforts

During the next quarter, TDWR data will be incorporated into the 3-D multi-radar mosaic algorithm, together with nearby WSR-88D data. The test will be carried out for a domain that covers Oklahoma and Texas Panhandle area, and the TDWR data will be from Oklahoma City (Will Rodgers) airport.

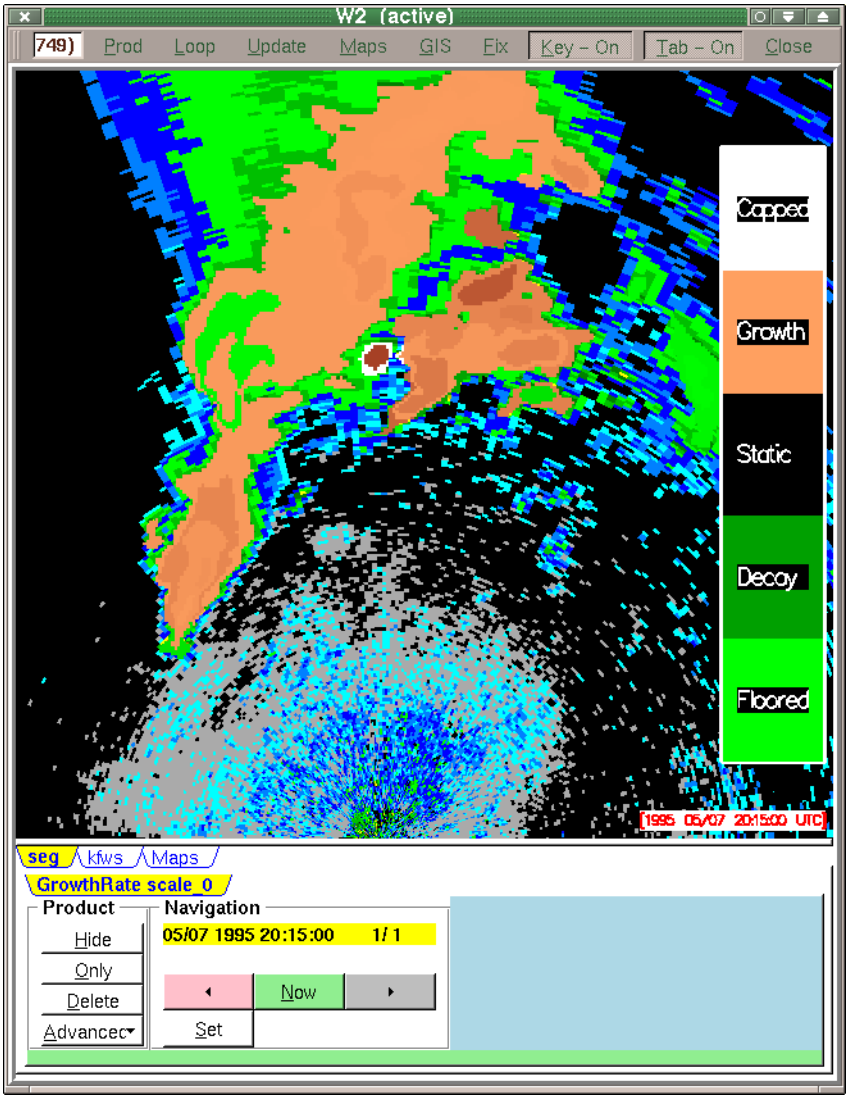


Figure 10. NSSL k-means-based growth and decay product overlaid on base reflectivity image.

c) Problems/Issues

Currently there is no access available to NSSL through any route for the TDWRs within CIWS. However, the task has been chanbged to allow development based on avaialble access to the Will Rogers (OKC) TDWR.

d) Interface with other Organizations

There have been communications between the NEPDT at NSSL and the MIT/LL regarding real-time TDWR data for the CIWS domain. NEPDT has been requesting access to those radars via LDM in real-time.

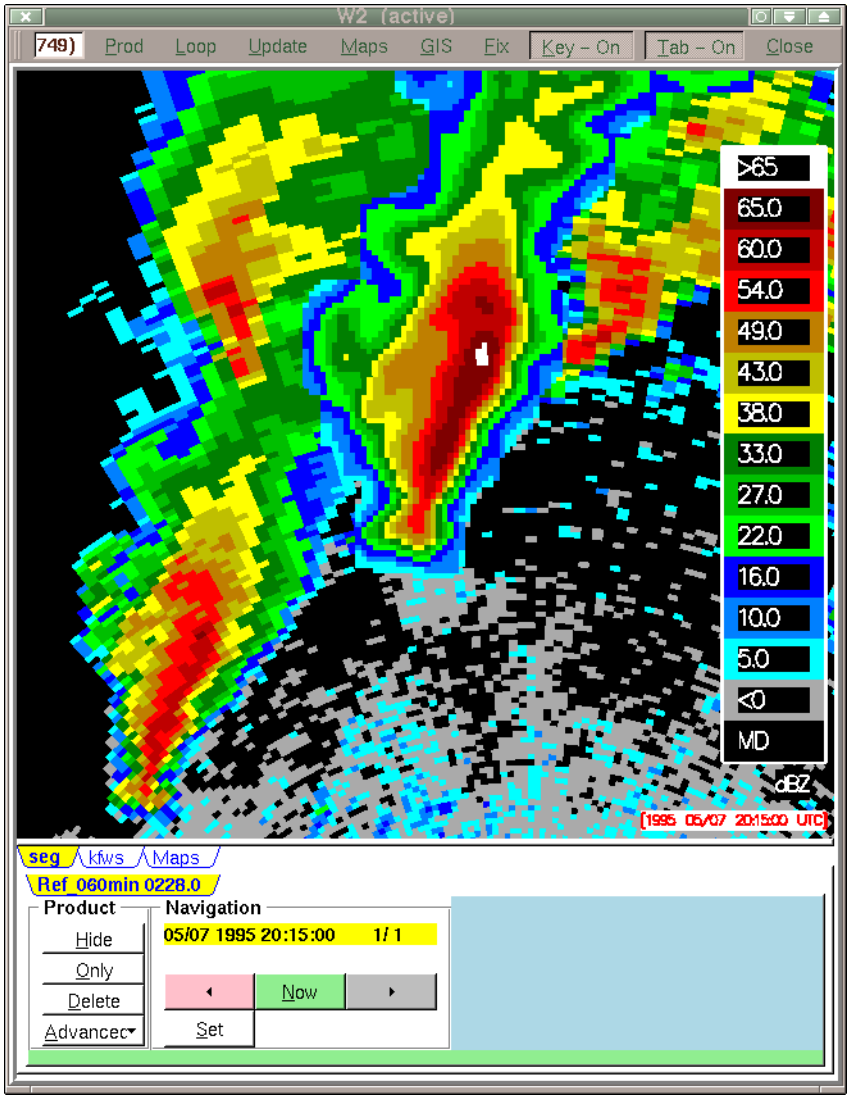


Figure 11. NSSL k-means forecast for storm growth overlaid on base reflectivity. The growth forecast is in the center of the figure.

e) Activity Schedule Changes

Schedule for 02.6.9.E1 has been postponed to 31 Aug 2002 (from 30 June 02). The delay was due to a moving-up of the date for 02.6.14.E6 (from 30 Sept 02 to 30 June 02)

## 02.6.11 Volume Coverage Patterns

*Volume Coverage Patterns - develop and implement new VCPs to meet the WSR-88D coverage needs of the aviation community and the AWR PDTs.*

a) Current Efforts

During this quarter, no new VCP data were collected.

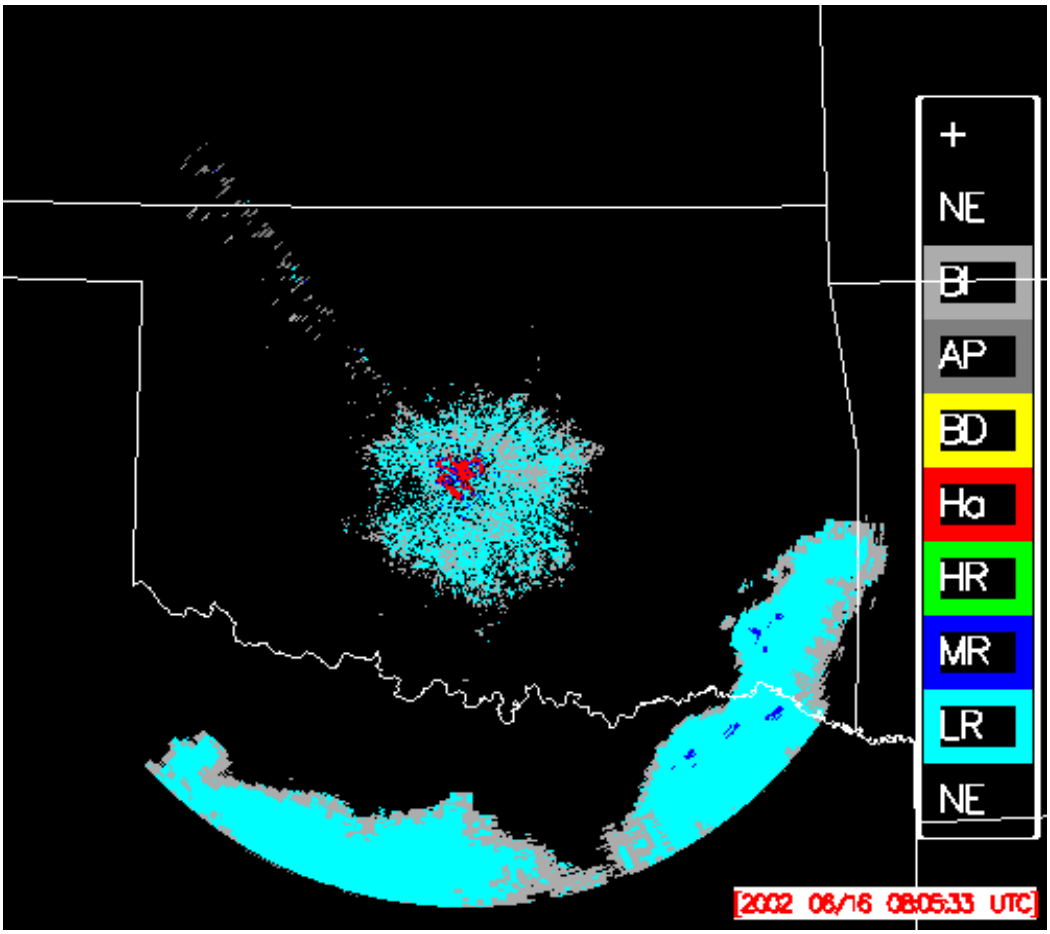


Figure 12. WDSS-II display of hydrometeor classification.

b) Planned Efforts

Continue analysis and data collection on new VCP's. In particular, check that current algorithms are compatible with new VCP's, and correct any incompatibilities.

c) Problems/Issues

None.

d) Interface with other Organizations

None.

e) Activity Schedule Changes

None

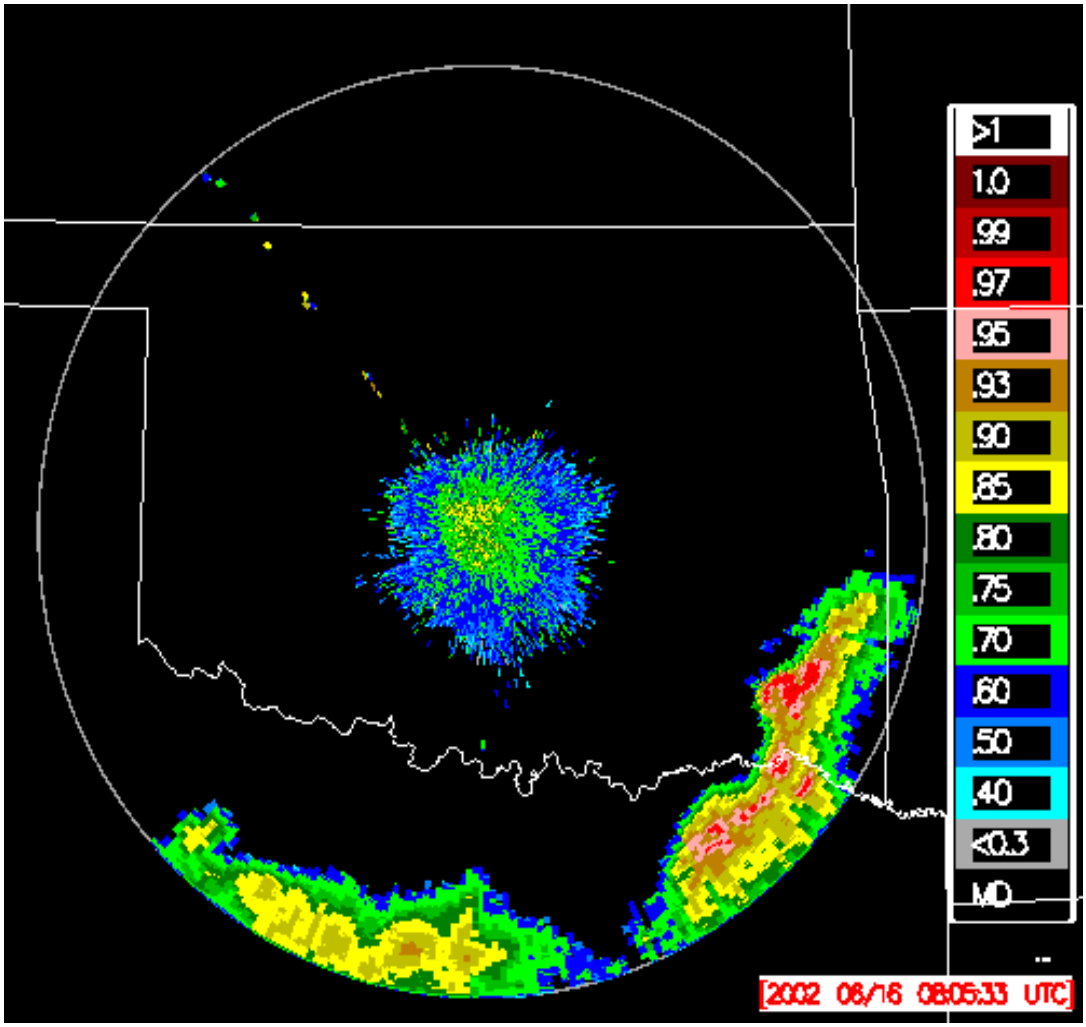

Figure 13. WDSS-II display of $\rho_{hv}$.

**02.6.12 Product Implementation**

*Explore and define aviation-specific products and implementation paths appropriate for NEPDT efforts.*

a) Current Efforts

New sea clutter rejection product development begun applicable to both polarimetric and non-polarimetrric radars.

b) Planned Efforts

Continue exploring current product applications and new product development specific to aviation needs.

c) Problems/Issues

None.

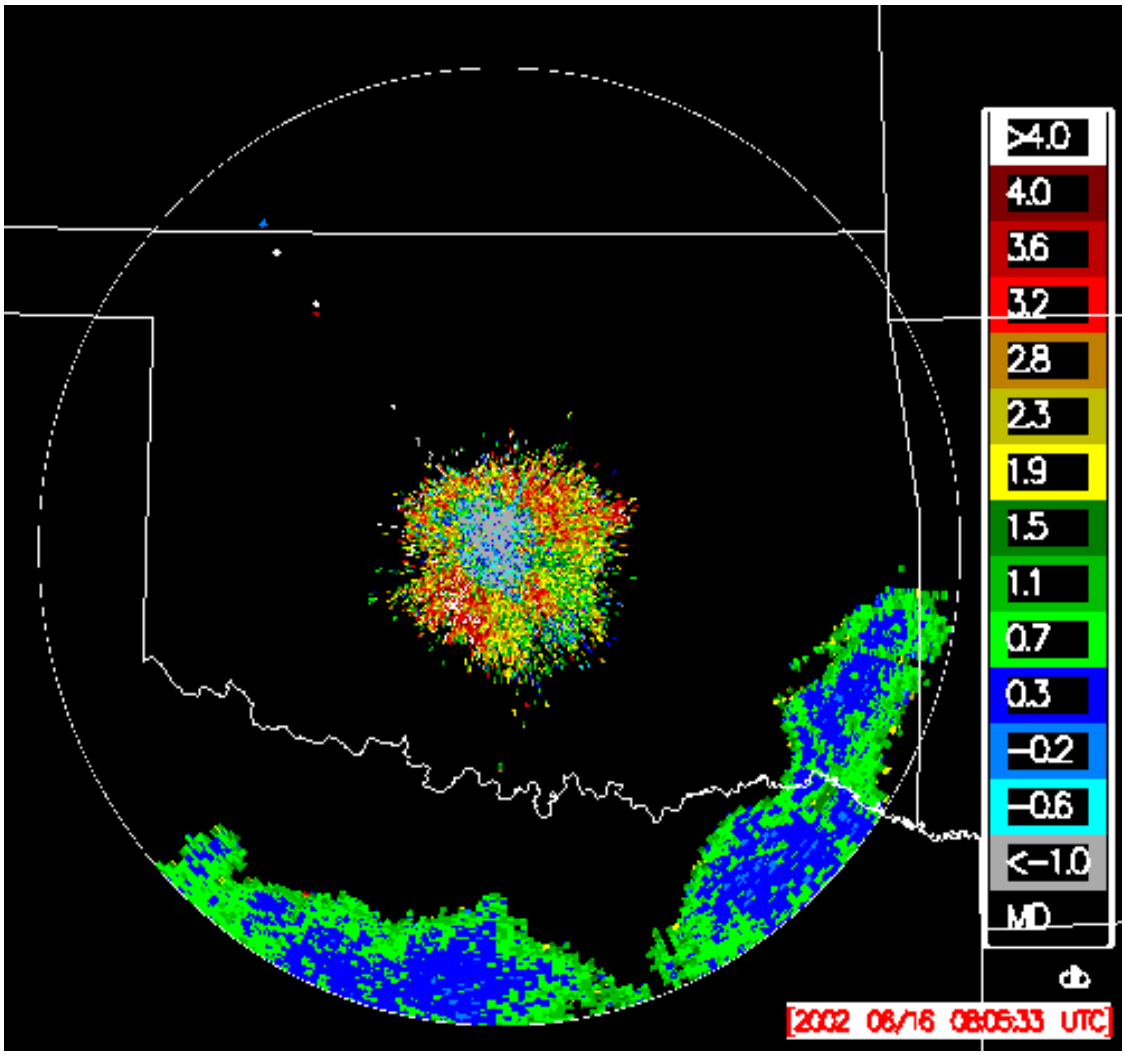

Figure 14. WDSS-II display of $Z_{dr}$.

d) Interface with other Organizations

None.

e) Activity Schedule Changes

None

**02.6.14 Multi-radar Composites**

*Examine aspects of multiple radar integration and algorithms.*

a) Current Efforts

02.6.14.5 Test different strategies for producing mosaic products using nested grid.

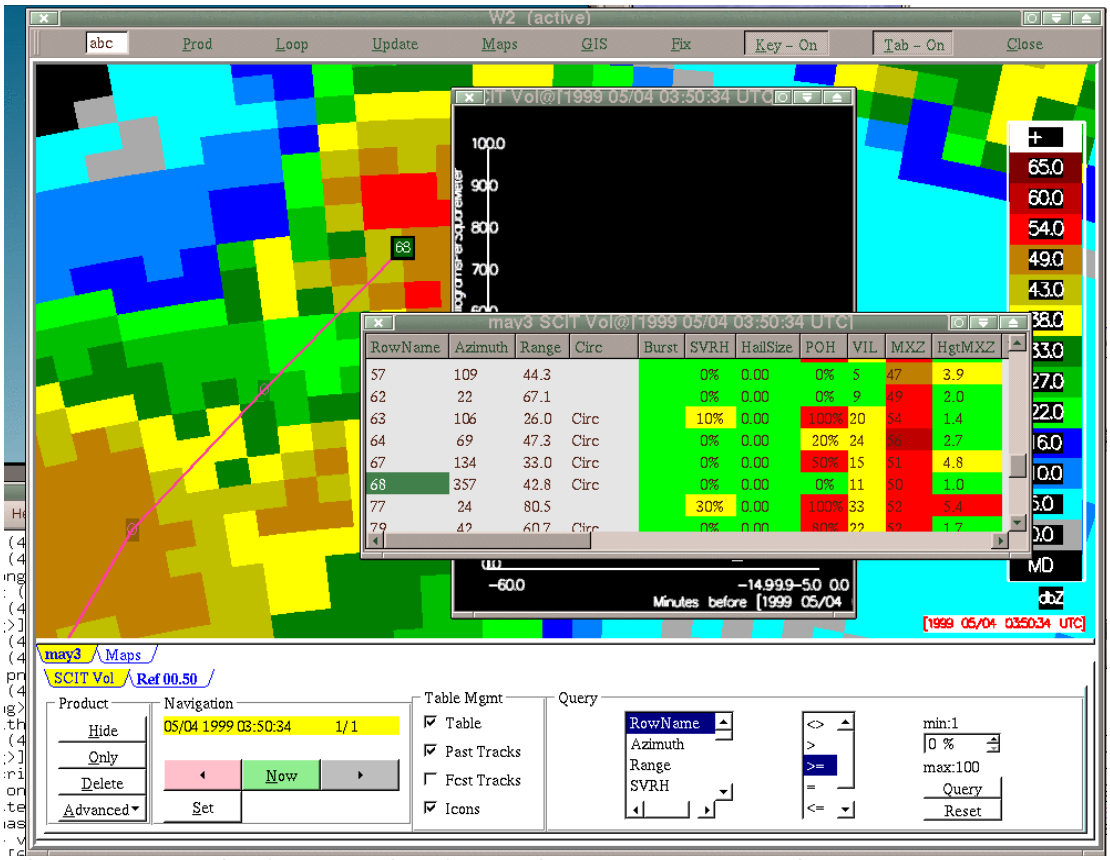

Figure 15. Example of WDSS-II interface and aaccess to LDM products.

The activities for this quarter include investigating and testing for the following two grid options for the CIWS domain: 1) using coarse resolution for big domains and fine resolution for small domains that are nested inside the big domains; 2) dividing a large domain into several sub-domains (tiles) with a single fine resolution.

The choice of the grid options depends on 1) applications, 2) data resolution, and 3) computational resources. Grid resolution should be comparable to data resolution so that storm structures observed in the data are represented well in gridded analyses. Applications may require very high spatial/temporal resolutions. But a very high-resolution grid mesh may not be useful if the resolution is much finer than what data could provide. Also, in an operational environment, computational efficiency becomes very important because fast updates are needed for warning decisions. This factor often limits the grid resolution that one could use for real-time products.

Both options can be used when a large region needs to be monitored and high-resolution analyses are wanted in real-time. If option 2 can be implemented for any given applications, then it is more advantageous than option 1 because it is easier to implement and to maintain, due to a unified grid resolution. The nested grids with different resolutions require more computer resources on data

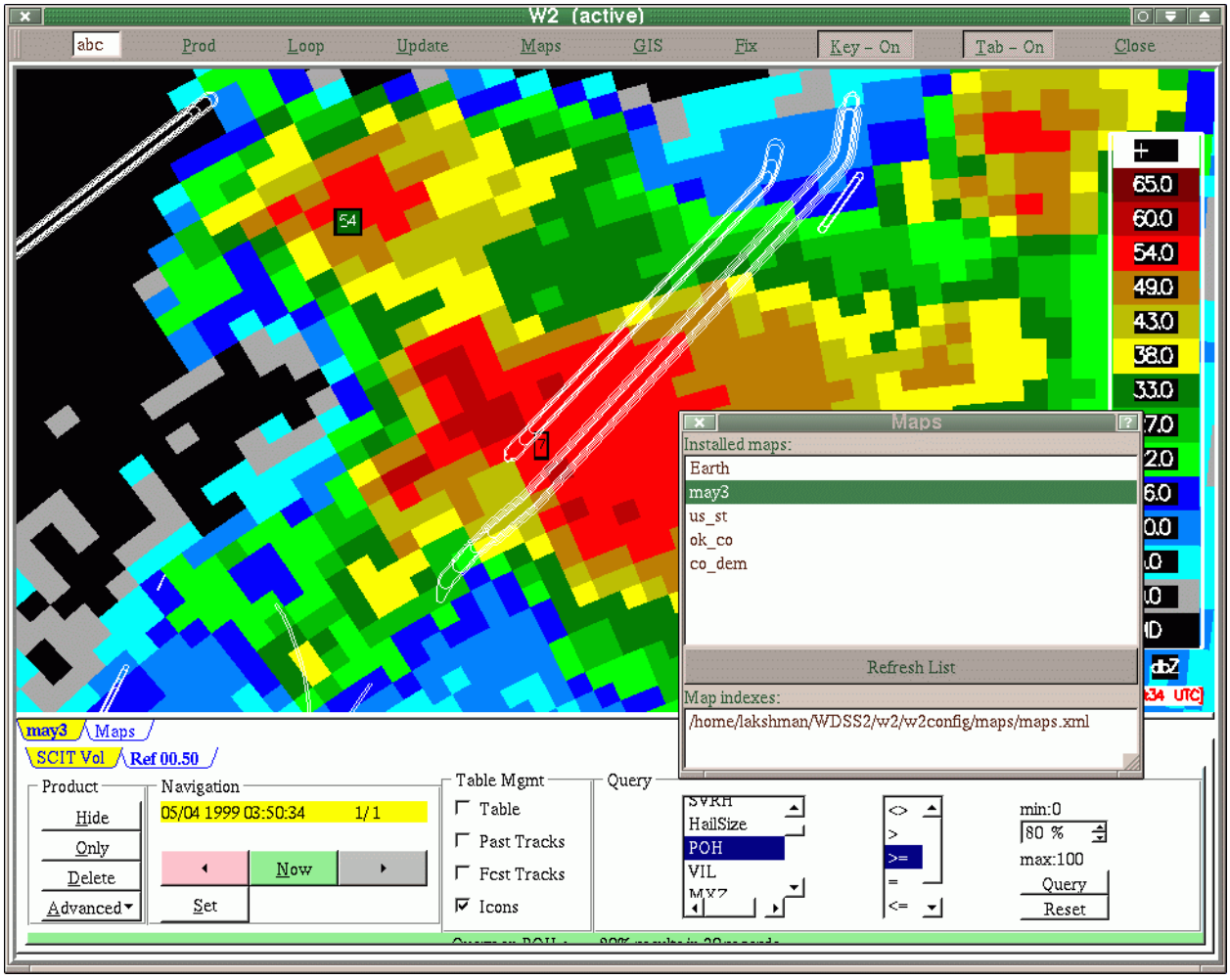


Figure 16. Ground truth (3 May 1999 tornado tracks) overlaid on base refelctivity.

and software control and management. However, if very high-resolution data are available only for small regions (e.g., TDWR data in vicinity area of an airport) and an application requires a very fine resolution grid (e.g., microburst detection), option 1 may be more suitable.

For the CIWS domain, the data currently available are some of the WSR-88Ds that cover the region. The WSR-88D data resolution is 1 km in range and variable in azimuth and elevation (approximately vertical) directions. Figures 1 and 2 show the radar data resolution in elevation direction (i.e., distances between centers of radar bins on adjacent tilts at the same range and same azimuth) for VCP 21 and VCP 11. The resolution is lower than 3 km (1km for VCP 11) beyond 50 km range at higher tilts. The resolution in azimuth direction (i.e., distances between centers of radar bins in adjacent radials at the same range and on the same tilt) is the same as the lines shown in Fig. 19 and Fig. 20 for tilt 1-2, 2-3, 3-4 and 4-5. So the resolution is worse than 1 km at ranges beyond 60 km. Based on these facts, a horizontal resolution of ~1 km was chosen for the

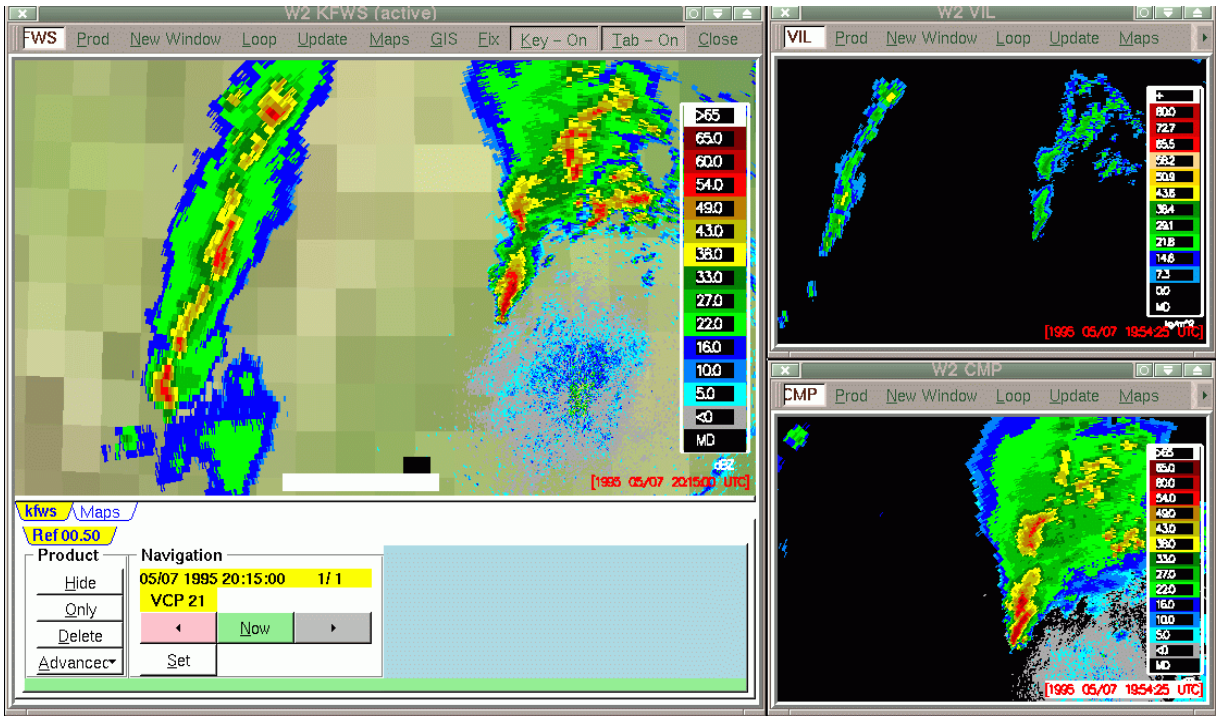


Figure 17. Example of WDSS-Ii multiple-window display.

3D mosaic for CIWS domain. The resolution is not exactly 1km because a equidistant cylindrical (constant latitude/longitude) projection is used for the 3D mosaic grid.

As mentioned above, the grid option 2 is relatively easier to manage than it is for option 1. The CIWS domain has been divided into 3 equally sized tiles (see NEPDT 1st quarter report for year 2002, task 02.6.14), and benchmark tests have been carried out to determine computational cost for the 3D mosaic. The results have shown that the 3D mosaic can be run efficiently for the 3 tiles with 1 km resolution and thus real-time operation is feasible (see NEPDT 2nd quarter report for year 2002, task 02.6.14), and option 2 has been chosen for running the real-time 3D mosaic for the CIWS domain.

02.6.14.6 Provide mosaic products for prototype display and refining the product data format based on requirement of display systems.

The activities for this quarter include setting up real-time data feeds via the Unidata LDM (Local Data Manager) software for all available radars in the CIWS domain. Table 1 lists the radars that are currently ingested at the NSSL. The level-II data from these radars are available from CAPS (Center for Analysis and Prediction of Storms) at the University of Oklahoma through CRAFT (Collaborative Radar Acquisition Field Test) network. Note that some radars cover more than one domains/tiles. There will be more radars available in the near

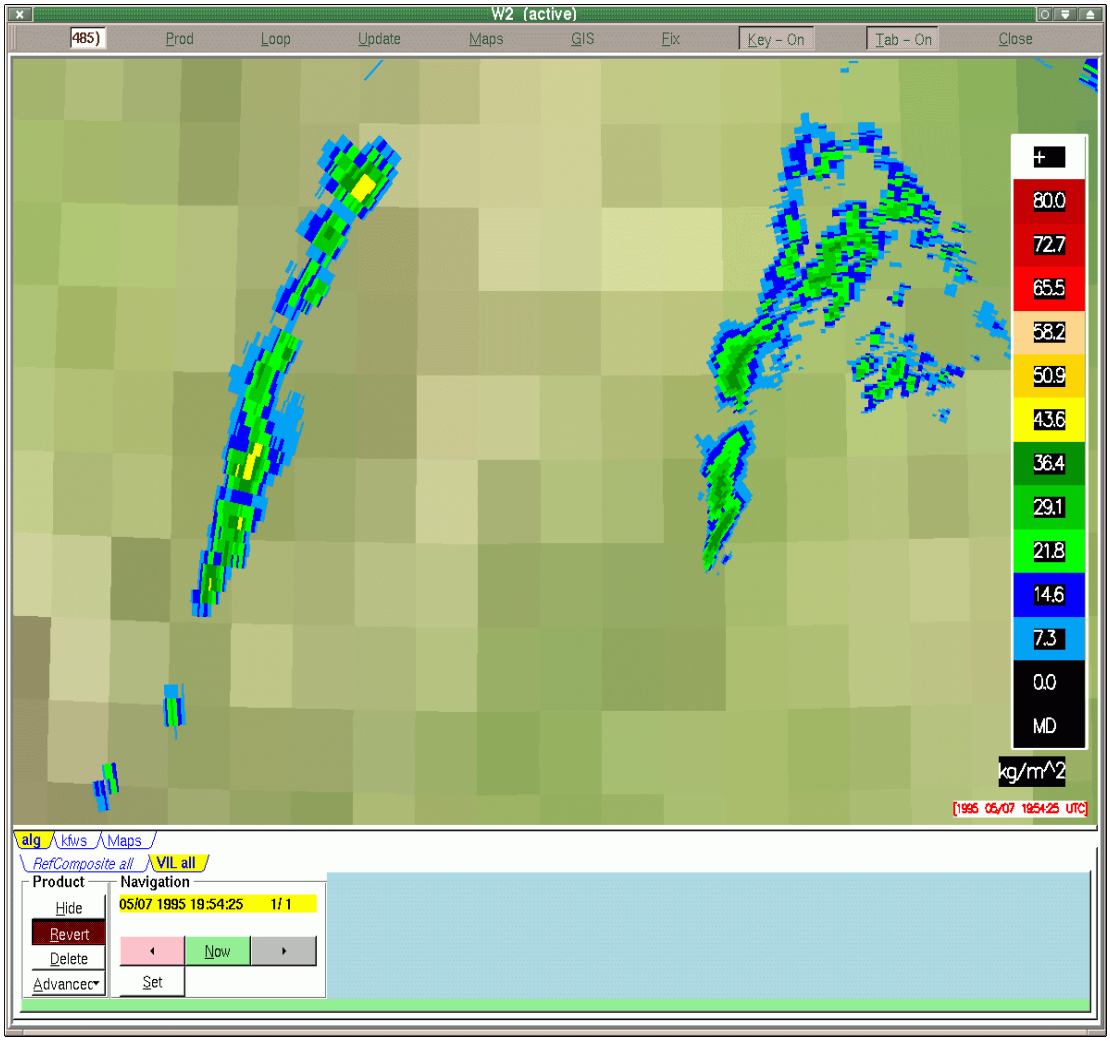


Figure 18. WDSS-II display of TWDR VIL.

future (personal communication, wolfson@ll.mit.edu, 2002) and those are listed in Table 2. Reference data sets, which include terrain, hybrid tilts, and conical-to-Cartesian coordinate transformation matrix, etc, have been established for all three CIWS tiles.

The 3D multi-radar reflectivity mosaic has been running in real-time for the CIWS_A domain, and prototype mosaic products have been generated in real-time. Example products are converted into NIDS data format and have been displayed in a web-based system. The products include composite reflectivity, height of composite reflectivity, cross sections of reflectivity on constant heights, and reflectivity on isothermal surfaces. Figures 21-23 show images of some example products. Other products, e.g., vertically integrated liquid (VIL) and center of VIL mass, can be derived if required.

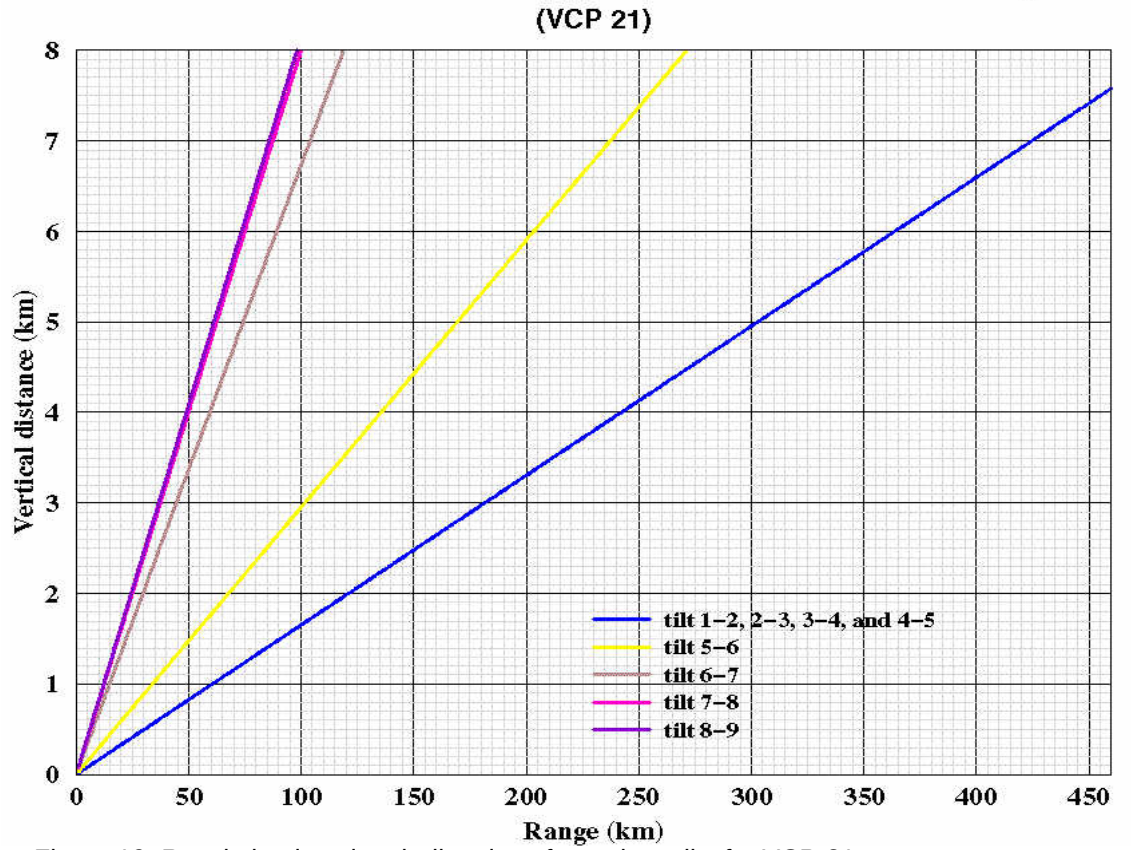

Figure 19. Resolution in azimuth directions for various tilts for VCP-21.

b) Planned Efforts

Develop product suites in NetCDF format. Purchase computers and setup initial configurations for running the 3D mosaic in real-time for the CIWS domain.

c) Problems/Issues

None.

d) Interface with other Organizations

None.

e) Activity Schedule Changes

None.

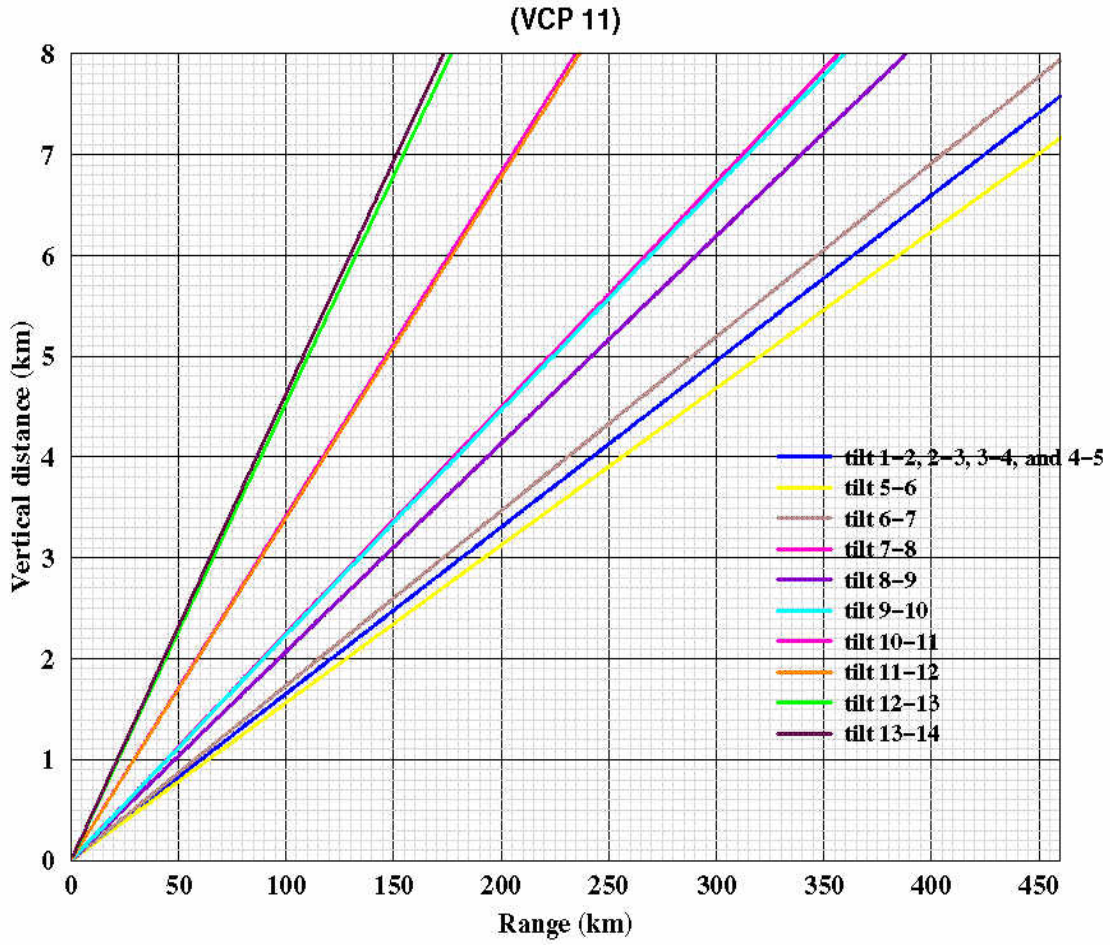


Figure 20. Same as Fig. 19, but for VCP-11.

**Table 1: List of the WSR-88Ds that are currently available at the NSSL for the CIWS domain.**

| CIWS_A | CIWS_B | CIWS_C |
|---|---|---|
| 11 radars | 17 radar | 10 radar |
| KCAE, KCLE, KDTX, KFFC, KGSP, KHTX, KILN, KIWX, KLOT, KOHX, KPBZ | KAKQ, KBMX, KBUF, KCAE, KCCX, KCLE,KDTX, KFFC, KGSP, KHTX, KILN,KIWX,KLTX, KMHX, KOHX, KPBZ, KRAX | KAKQ, KBUF, KCAE, KCCX, KCLE, KLTX, KMHX, KOKX, KPBZ KRAX |

**Table 2: List of the WSR-88Ds that will be available to CAPS from MIT/LL.**

| CIWS_A | CIWS_B | CIWS_C |
|---|---|---|
| 9 radar | 7 radars | 6 radars |
| KBMX, KDVN, KILX, KIND, KLSX, KLVX, KMKX, KPAH, KRLX | KBGM, KDIX, KENX, KIND, KLVX, KLWX, KRLX | KBGM, KBOX, KDIX, KENX, KLWX, KRLX |

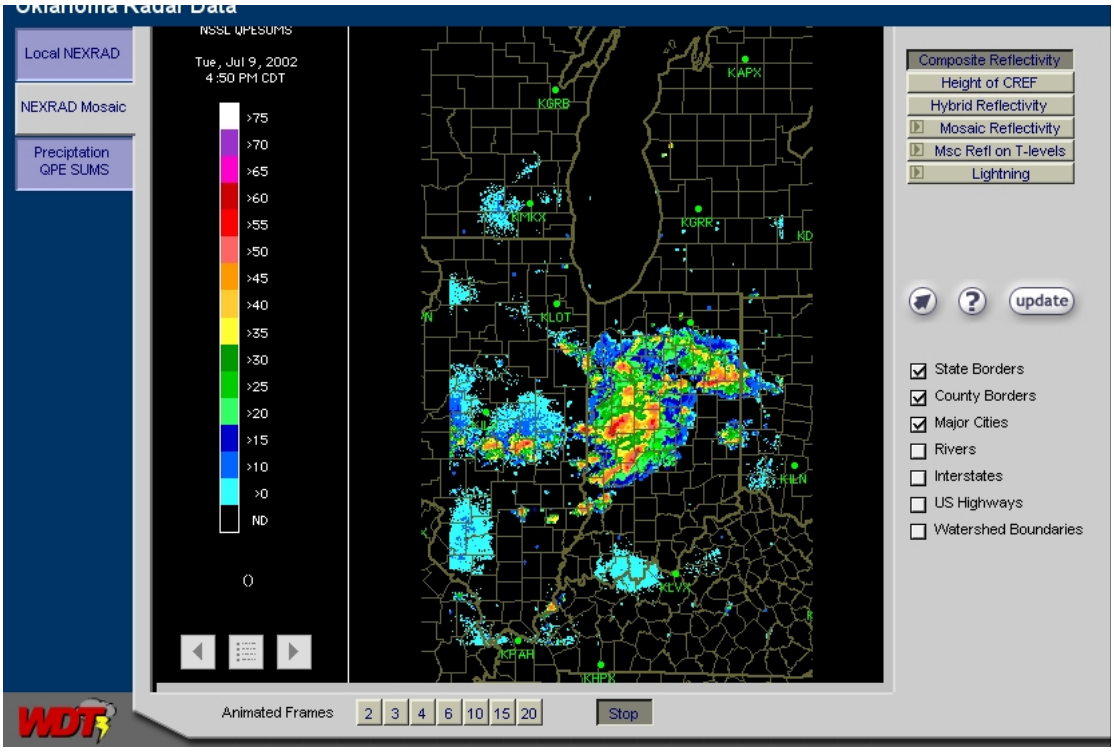


Figure 21. Real-time composite reflectivity image from CIWS_A domain at 4:50pm CDT on 9 July 2002.

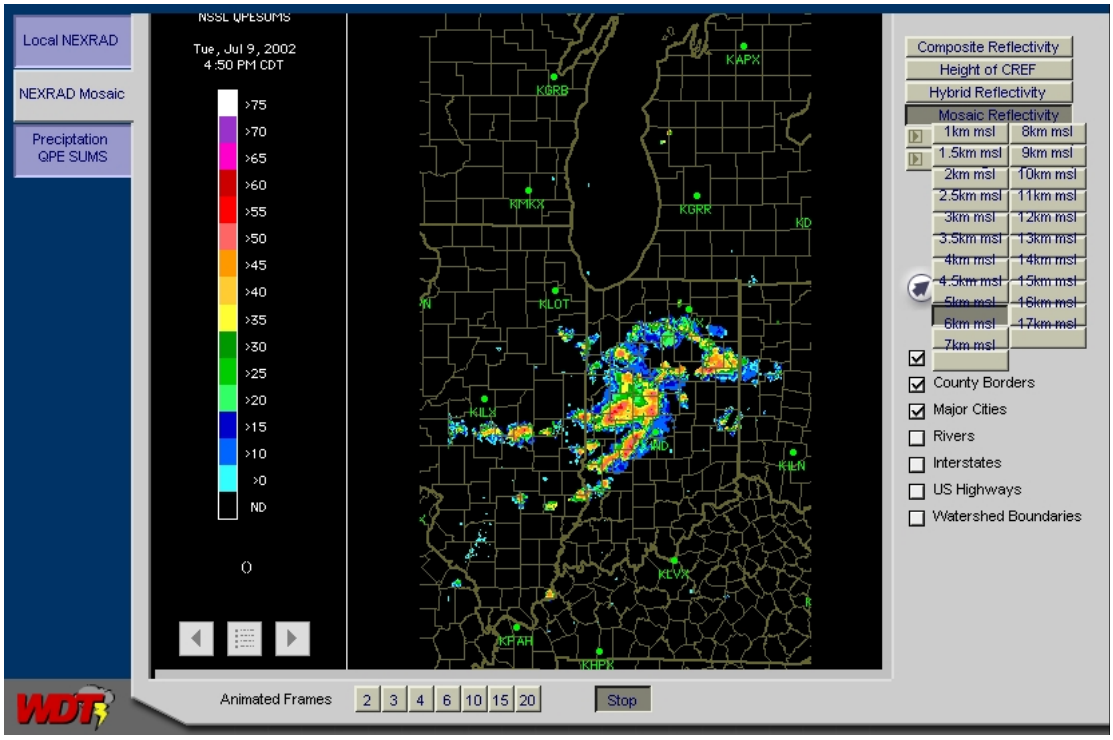


Figure 22. Same as in Fig.3 except for horizontal cross section of the mosaicked reflectivity field at 5 km msl.

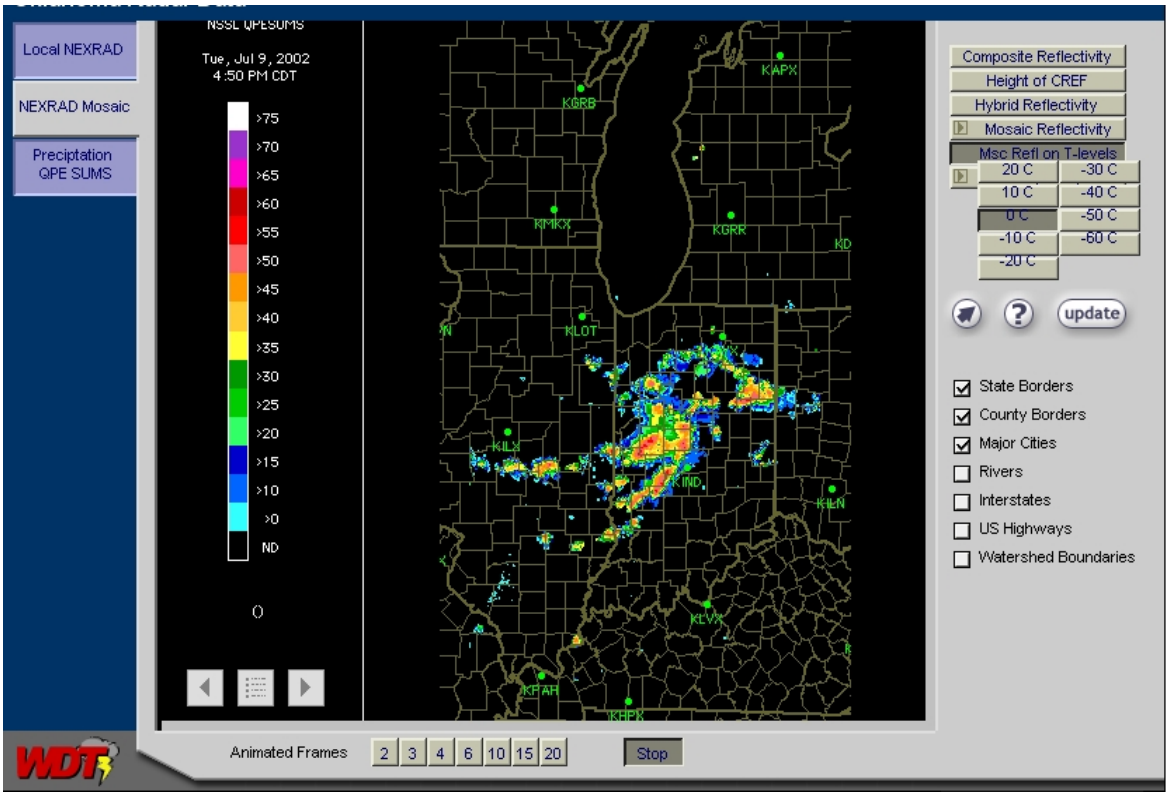


Figure 23. Same as in Fig.4 except for the layer mosaicked reflectivity field on 0°C isothermal surface.

**02.6.15 WARP Activities**

*Develop strategies and algorithms to remove meteorologically insignificant artifacts; develop next-generation WARP products, based on multi-radar gridded data, suitable for display to air traffic controllers.*

a) Current Efforts

Four different anomalous propagation (AP) events are being analyzed currently as part of the evaluation of Unisys' anomalous propagation (AP) mitigation algorithm developed for WARP. AP cases being studied include nocturnal AP, AP co-existent with but not embedded within convection, AP embedded within a mesoscale convective system, and sea clutter. Steiner and Smith (2002) provide analysis of the last three types of AP currently being studied. Subjective analyses of all cases are being performed to produce truth files that identify regions of AP versus precipitation. This allows for a quantitative analysis calculating the percentage of AP and precipitation returns that are removed from the radar display.

The nocturnal AP case occurred April 18, 2002 surrounding the Amarillo, TX WSR-88D radar. Intense reflectivity values greater than 65 dBZ exist southwest of the radar (Figure 24) and certain regions of AP returns are difficult to

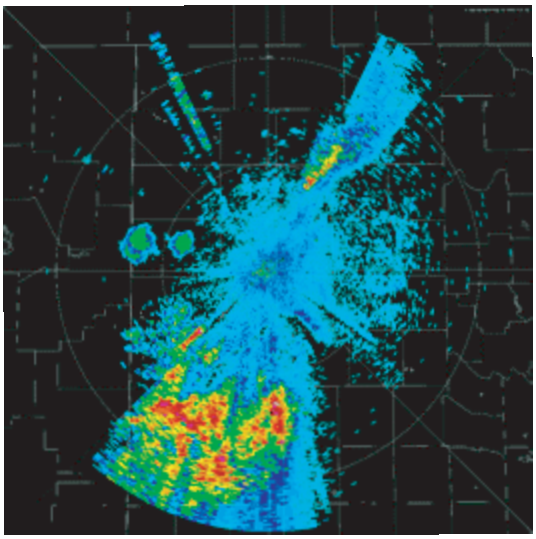

Figure 24. KAMA WSR-88D base reflectivity (ORPG product 19) valid at 0719 UTC 18 April 2002.

remove (Figure 25). Dave Smalley of Lincoln Labs provided the two figures shown. The low-layer composite reflectivity product anomalous propagation removed product (ORPG - product 97) is not able to remove all AP returns approximately 150 km southwest of the radar (Figure 2). This strongly influences the Unisys AP mitigation scheme since it is heavily dependent on product 67 (a 4 km version of ORPG product 97). A quantitative analysis of how much AP is removed in this case is being performed at this time. This AP event

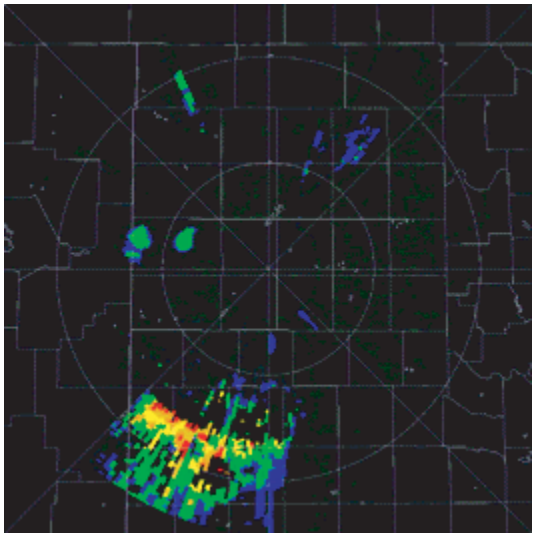

Figure 25. Same as Fig. 24 but for 1 km composite reflectivity with ORPG 1.2 default adaptable parameters settings fpr AP removal.

probably represents an extreme nocturnal case and is likely not indicative of how the AP mitigation scheme typically performs in nocturnal AP events.

ORPG software has been successfully installed on a Linux machine to provide input files for the Unisys software.

b) Planned Efforts

Continue progress with truthing process.

c) Problems/Issues

None.

d) Interface with other Organizations

None.

e) Activity Schedule Changes

None.